NPC Photovoltaic Grid-Connected Inverter with Ride-Through Capability under Grid Faults

Hossein Dehghani Tafti[1], *Student Member*, *IEEE*, Ali I. Maswood[2], *Senior Member*, *IEEE*, Ziyou Lim[3], *Student Member*, *IEEE*, Gabriel H. P. Ooi[4], *Member*, *IEEE* and Pinkymol Harikrishna Raj[5], *Student Member*, *IEEE*.

[1, 2, 4, 5]School of Electrical and Electronic Engineering, Nanyang Technological University, Singapore

[3]Energy Research Institute @ NTU (ERI@N), Interdisciplinary Graduate School, Nanyang Technological University, Singapore

Email: [1]hossein002@e.ntu.edu.sg, [2]eamaswood@ntu.edu.sg

***Abstract*—Fault ride through (FRT) capability is one of the challenges faced in the medium to high voltage grid-tied large-scale photovoltaic (PV) power plants. This paper proposes a novel control strategy to enhance the FRT capability of a two-stage multi-string PV plant which consists of DC/DC converters and NPC inverter. The proposed control is implemented to the DC/DC converter to maintain the DC-link voltage under any grid fault conditions by adjusting the extracted PV power to the inverter output power. This is achieved by changing the PV string reference voltage from its maximum power point voltage to a new voltage point with less power. On top of that, a novel voltage-oriented control (VOC) control structure using proportional-resonant (PR) controller is proposed for the NPC inverter. Additionally, the DC-link capacitor voltages are remained balanced at all times due to the adaptive space vector modulation (ASVM) scheme. The evaluation results have verified the feasibility and the FRT capability of a 14kW PV plant using the proposed control scheme under different grid fault conditions.**

***Index Terms*—Photovoltaic systems, adaptive space vector modulation, voltage oriented control, proportional resonant control, Fault Ride-Through capability, NPC inverter.**

I. INTRODUCTION

Large-scale photovoltaic (PV) power plants are one of the most promising renewable sources for electricity generation nowadays which have gained significant growth over the recent years. Such rapid pace for the total installed PV capacity growth is initiated due to the drastic decrease of the PV panel production cost and is expected to remain high in the upcoming years. Since these large-scale PV power plants are typically connected to the medium voltage (MV) or high voltage (HV) systems, the grid-connected power converters in the renewable systems often pose new challenges for the power system operators (PSOs). Therefore, certain regulations and grid codes are imposed by PSOs to deliver excellent power quality as well as maintain high grid reliability [1], [2]. One of the challenges is fault ride-through (FRT) capability of these renewable power plants. Hence, it is important to investigate the FRT capability of the large-scale PV grid-connected power plants under any grid faults.

Several research studies on the FRT capability of the single-stage PV power plants have been reported and investigated [3]-[5]. For the single-stage PV power plants configuration, the PV strings are directly connected to the DC-link of the grid-tied inverter without any DC/DC conversion stage. In this case, the maximum DC-link voltage (V_{dc}) will be the open-circuit voltage of the PV strings. Thus, no additional DC voltage control is needed when any fault condition occurs.

On the other hand, the two-stage PV plants (which consist of DC/DC converters and multilevel inverters) are popularly known as the state of the art today, due to their perceived advantages in achieving higher energy conversion efficiency, modularity and power density [6], [7]. However, there are several problems faced in this two-stage structure when grid fault conditions are identified.

In the event of the grid voltage sag condition, the decreased in the grid voltage will cause an increase in the inverter output current due to the power balanced principles. As a result, the semiconductor switches may be overheated or damaged. If the grid-tied inverter of the two-stage PV power plants decreases the amount of active power injected to the grid ($P_{O.Inv}$) while the DC/DC converters continue to extract the maximum power ($P_{st.Total}$) from the PV strings, the excessive energy which is the difference power ($P_{st.Total}$ - $P_{O.Inv}$) between the extracted PV power and the injected grid power will be stored in the DC-link capacitors. This will lead to an increase in the V_{dc} and may unbalance the DC-link capacitor voltages. The output voltages total harmonic distortion (THD) and the system reliability are both greatly affected as well.

In this study, the two-stage multi-string PV power plant consisting of simple DC/DC boost converters and a neutral point-clamped inverter (NPC) is considered. This paper proposes a DC-link voltage control strategy for the DC/DC boost converter which addresses the aforementioned challenges

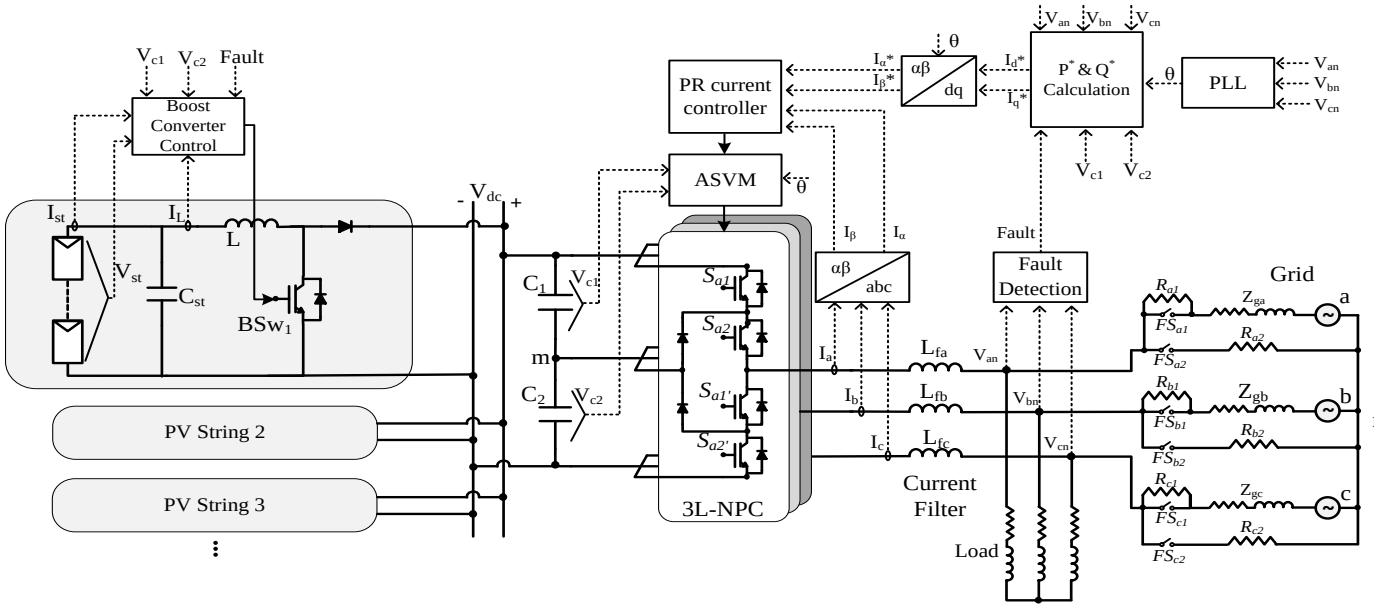

Fig. 1: Multi-string PV power plant with FRT capability.

by reducing the amount of $P_{st.Total}$ to match with the instantaneous $P_{O.Inv}$. On top of that, a novel voltage-oriented control (VOC) consists of proportional-resonant controller (PR) and adaptive space vector modulation (ASVM) is proposed for this system. The proposed VOC controls the injected active and reactive power to the grid when fault conditions are experienced, meanwhile the DC-link capacitor voltages are balanced at all times. The evaluation results have verified the FRT capability of the system using the proposed control strategy under various grid faults. On top of that, the behaviour of the PV system is examined in the open loop to highlight the improvements made from the proposed control structure.

II. Proposed System Structure

A comprehensive structure of the proposed multi-string PV system with FRT capability depicted in Fig. 1 consists of multiple PV strings, DC/DC converters and NPC inverter. Since each PV string is working independently, different types of PV panels or DC/DC converter topologies can be utilized as well for the proposed configuration. Hence, a simple DC/DC boost converter is connected to each PV string in this study.

The grid-tied NPC inverter consists of two pairs of IGBT switches (S_{a1} and S_{a2}) including their complementary ($S_{a1'}$ and $S_{a2'}$) in each phase-leg. There are filter inductors connected in between the inverter and the grid to provide low current THD performance at all times to comply with both grid codes and IEEE standards [8].

There are different operating modes (on/off) for the switches FS_{a1} and FS_{a2} in Fig. 1 to stimulate different grid fault conditions. Under a normal operation, the load is directly connected to the voltage source with the FS_{a1} switched on and FS_{a2} switched off. To create a voltage sag in the phase A, both FS_{a1} and FS_{a2} will be switched off and on respectively. Hence, the values of the resistors R_{a1} and R_{a2} are selected accordingly to generate the desired voltage sag level.

III. Proposed Control Strategy

Based on the grid condition (normal operation or fault occurrence), suitable control strategy should be designed appropriately for the multi-string PV power plant. Therefore, a fast and precise sag detection strategy is required in the controller. In this proposed system, the voltage sag is detected by monitoring the peak value of the grid voltages which can be calculated based on the T/4 delay orthogonal method [9], [10]. The system is operating under two independent control strategies which are the DC/DC converter controller and the NPC inverter controller. These controllers as well as grid requirements under fault condition are presented in the following subsections.

A. Grid requirements under fault condition

The grid reactive current requirements for a distributed generator (DG) under various grid faults are depicted in Fig. 2. The amplitude of the voltage between 0.9 p.u. and 1.1 p.u is defined as normal grid condition. When there is no grid fault condition, the DG injects only the active power to the grid with unity power factor. According to this regulation, the DG should support/limit the grid voltage during voltage sag/swell by

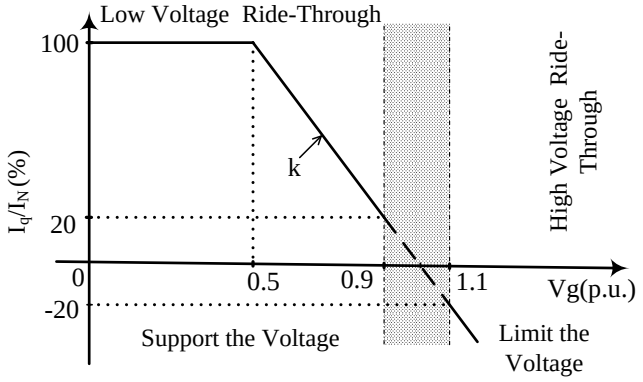

Fig. 2: Grid Reactive current requirement in various grid conditions

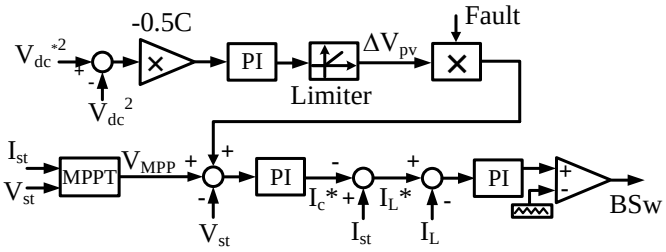

Fig. 3: Proposed DC/DC boost converter control structure under grid faults.

injecting/consuming the reactive power. Therefore, the DG cannot inject its maximum power to the grid due to restricted current capability of the inverter.

According to the regulated grid codes (Fig. 2), the amount of the reactive current that should be injected to the grid during voltage sag is defined in the following:

$$I_q = \begin{cases} \text{deadband} & 0.9\text{p.u.} \le V < 1.1\text{p.u.} \\ k.\dfrac{V\text{-}V_0}{V_N}.I_N + I_{q0} & 0.5\text{p.u.} \le V < 0.9\text{p.u.} \\ -I_N + I_{q0} & V \le 0.5\text{p.u.} \end{cases} \quad (1)$$

where V, V_0 and V_N are the amplitude values of the grid instantaneous voltage, the initial voltage before the fault, and the nominal grid voltage respectively. I_N and I_{q0} are the nominal current and the initial reactive current before the grid failure respectively while $k = (\Delta I_q/I_n)/(\Delta V/V_n)$ [11].

The amount of d-axis current can be calculated using (2) assuming that the PV system is operating at its nominal power.

$$I_d = \sqrt{I_N{}^2 - I_q{}^2} \quad (2)$$

B. Proposed DC/DC converter controller under grid faults

Under normal grid operation, the MPPT controller adjusts the output voltage of each PV string (V_{st}) to its maximum power point voltage (Fig. 1) to extract the maximum power from the PV strings. In this situation, the V_{dc} is maintained only by the rear-end NPC inverter at its desired value by adjusting the reference d-axis current (I_d^*) which is related to the output active power ($P_{O.Inv}$) [12]. The reference q-axis current (I_q^*) which relates to the output reactive power is set to be zero in order to achieve the unity power factor operation under normal operation [13].

However, during the grid fault condition, the NPC inverter is responsible for controlling its output active and reactive power according to (1) and (2). Thus, the V_{dc} cannot be maintained and controlled solely by the inverter under any grid faults. Thus, this paper proposes a DC-link control strategy (Fig. 3) for the DC/DC boost converter. This proposed control will decrease the $P_{st.Total}$ to the instantaneous $P_{O.Inv}$ in the event of grid faults. The ΔV_{pv} is computed based on the difference between the square of the reference ($V_{dc}{}^{*2}$) and the instantaneous DC-link voltage ($V_{dc}{}^2$). The obtained ΔV_{pv} is then added to the V_{MPP} when there is any occurrence of grid faults. The PV string reference voltage will increase to its open circuit voltage and decrease the $P_{st.Total}$.

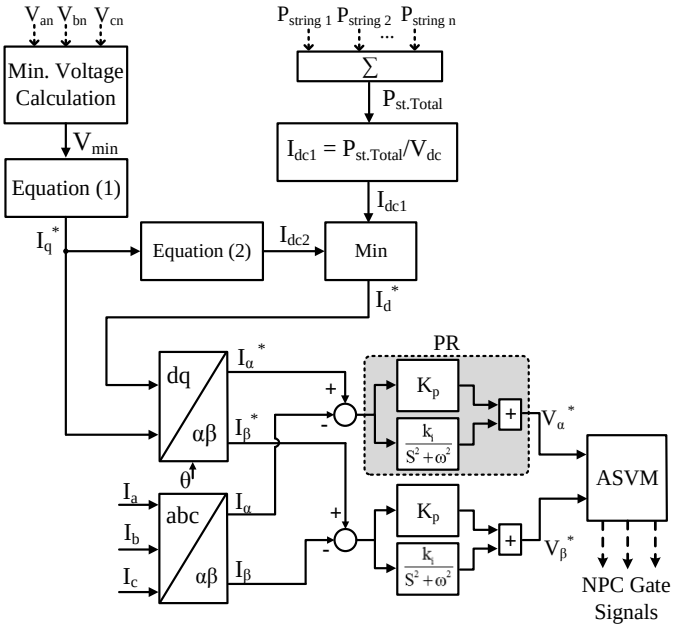

Fig. 4: Proposed VOC-PR control structure under grid faults.

The well-known Perturb and Observe (P&O) algorithm [14] is applied in this study. The calculated reference voltage, after adding ΔV_{pv} and V_{MPP}, is compared with the instantaneous voltage of the PV string while the difference goes through the PI controller which will generate the reference capacitor current ($I_{Cst}{}^*$). The inductor current can be written as:

$$I_L = I_{st} - I_{Cst} \quad (3)$$

Subsequently, by controlling the inductor current via a PI controller, the reference inductor voltage ($V_L{}^*$) is obtained. Lastly, the switching signals of the IGBT BSW1 are generated by comparing $V_L{}^*$ with a triangular high frequency signal.

C. Proposed VOC-PR controller under grid faults

After detecting the voltage sag by monitoring the grid voltage amplitude, the NPC controller should be changed in order to control its output reactive current according to the voltage sag level and (1). As depicted in Fig. 4, the minimum amplitude of three phase grid voltages are needed to determine the $I_q{}^*$. The reference active current (I_{dc2}) is then computed based on (2).

As mentioned earlier, this reference current is obtained only when the PV system is operating at its nominal value. However, the PV strings may experience partial shading. As a result, the total generated power of the PV power plant ($P_{st.Total}$) will be smaller than its nominal value. In this condition, the NPC inverter cannot inject I_{dc2} to the grid. To solve this problem, the total extracted power of all PV strings is calculated simultaneously using V_{st} and I_{st}. Hence, the related active current (I_{dc1}) is computed based on the DC-voltage. Subsequently, the $I_d{}^*$ is obtained based on the minimum value of I_{dc1} and I_{dc2}.

With the aid of inverse Park and Clarke transformations, the respective α-β current errors are obtained by subtracting the reference stationary frame currents ($I_\alpha{}^*$ and $I_\beta{}^*$) with the stationary frame currents (I_α and I_β). Hence, the reference

stationary frame voltages (V_α^* and V_β^*) which is fed into the ASVM can be acquired directly from the proportional resonant (PR) controller. The PR controller is proven for its fast dynamic response and reduced steady state error. It can eliminate the steady state reference error by having its resonant frequency matching with the grid frequency [15].

The implementation of the ASVM in the control for the system provides good DC-link capacitor voltages balancing since there are several pairs of vector to generate the same output voltage level for the NPC inverter [16]. However, each vector pair has an opposite effect in charging or discharging of the DC-capacitors (C_1 and C_2). According to the capacitor voltages (V_{c1} and V_{c2}) and inverter current (I_a, I_b or I_c) direction, the ASVM selects the appropriate vector to maintain the capacitor voltage at half DC-link voltage ($V_{dc}/2$) [17]. Since the voltage balancing operation of the ASVM is independent of the grid voltage, it can achieve voltage balancing in all of the grid operation conditions including unbalanced grid faults.

IV. Evaluation Results

The proposed multi-string PV plant (14kW) in Fig. 1 is modelled and developed using Matlab/Simulink© and PSIM. Three parallel PV strings are connected to the DC-link of the grid-tied NPC inverter to investigate the performance and the FRT capability of the proposed system under different irradiance, temperature and grid fault conditions. Each panel is simulated following the SHARP NUU235FI parameters with the maximum power of *235W* (*30V* and *7.84A*) at *25ºC* and *1kW/m²*. The detailed setting of the simulated system is presented in table I.

Since the grid voltage is $400V_{l\text{-}l,rms}$, the nominal dc-link voltage can be calculated according to (4) which is equal to $770V_{dc}$, considering a normal modulation index of 0.85 m_a.

$$V_{l-l,rms} = \frac{\sqrt{3}}{\sqrt{2}} \times m_a \times \frac{V_{dc}}{2} \qquad (4)$$

On the other hand, based on the boost converter equations, the maximum number of series connected PV panels in each string can be calculated in the following:

$$V_{st,max} = N_{panel,max} \times V_{panel,oc} \le 0.9 \times V_{dc} \qquad (5)$$

where $N_{panel,max}$ is the maximum number of PV panels which can be series connected in one string and $N_{panel,oc}$ is the open circuit voltage of a PV panel. According to (5), the $N_{panel,max}$ will be 23.1 but only 20 series-connected PV panels in a PV string is considered in this paper. Different amounts of irradiance and temperature are experienced by the PV strings where string I (*Irrad=1kW/m², Temp=25ºC*), String II (*Irrad=0.5kW/m², Temp=25ºC*) and String III (*Irrad=1.1kW/m², Temp=35ºC*).

The behaviour of the multi-string PV system is examined under three phase grid fault (V_{sag} = 30%) without applying the proposed DC/DC controller in Fig. 5. In this condition, the inverter produces reactive power for the grid according to (1) while the injected active power is zero as shown in Fig. 5(b). On the other hand, the DC/DC converters continue to extract the maximum power from the PV stings. However, the NPC inverter is controlling its output reactive power based on the grid requirements. Since $P_{O.Inv}$ is smaller than $P_{st.Total}$, the extra energy will be stored in the DC-link capacitors. Therefore, the DC-voltage is increased from 770V to more than 3500V as shown in Fig. 5(a) which will trigger the DC-voltage protection breaker. Besides that, it can be seen that both DC capacitors are well balanced at all times due to the ASVM voltage balancing technique implemented.

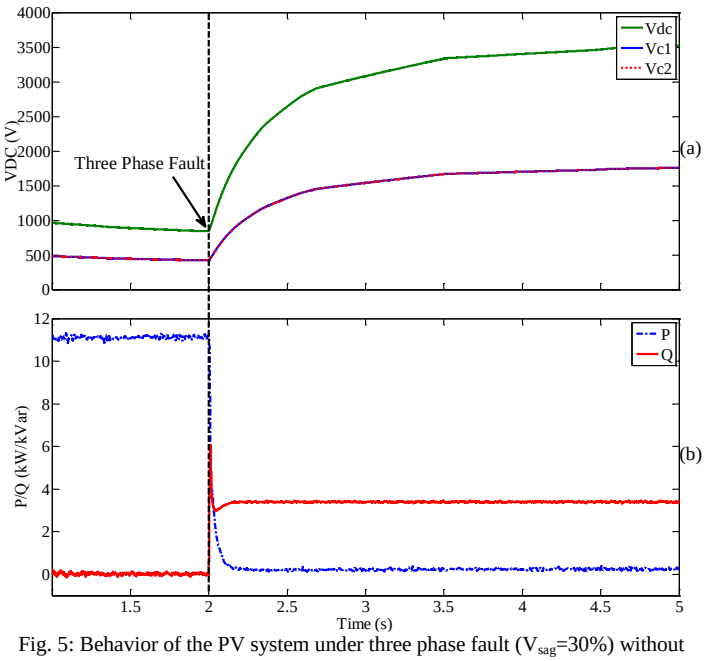

Fig. 5: Behavior of the PV system under three phase fault (V_{sag}=30%) without using proposed DC/DC controller: (a) DC-link voltage and (b) Injected active/reactive power to the grid.

TABLE I
Simulation Parameters

Parameter	Symbol	Value
Grid Voltage	V_{ab}	400 $V_{l\text{-}l,rms}$
Grid Frequency	f	50Hz
Line Inductor	L_f	5mH
DC-link Capacitor	C_1 , C_2	2200µF
DC-link Voltage	V_{dc}	770 V_{dc}
NPC Switching Frequency	$f_{s,inv.}$	7.2kHz
Boost Switching Frequency	$f_{s,boost.}$	10kHz
Boost Inductor	L	1mH

In order to investigate the FRT capability, there are two different grid fault conditions modelled as shown in Fig. 6. The first grid fault condition (Cond. I) shown in the Fig. 6(a) occurred between 5s to 6s where the three phase voltages sag level of 87%. The second condition (Cond. II) in Fig. 6(b) will be the unbalanced two-phase to ground fault (AB-G) during 7s to 8s with phases A and B voltages sag level of 40%.

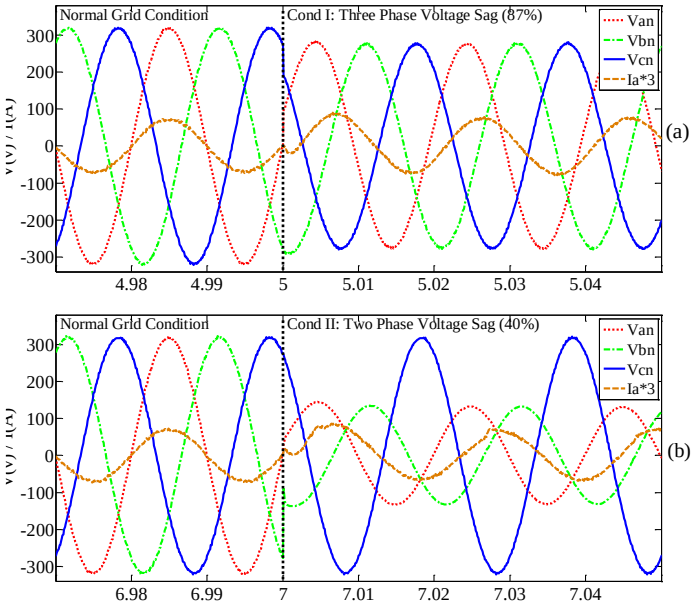

Fig. 6: Three phase grid voltage and phase A current (a) Cond. I: Three phase voltage sag (87%) and (b) Cond. II: Two phase voltage sag (40%).

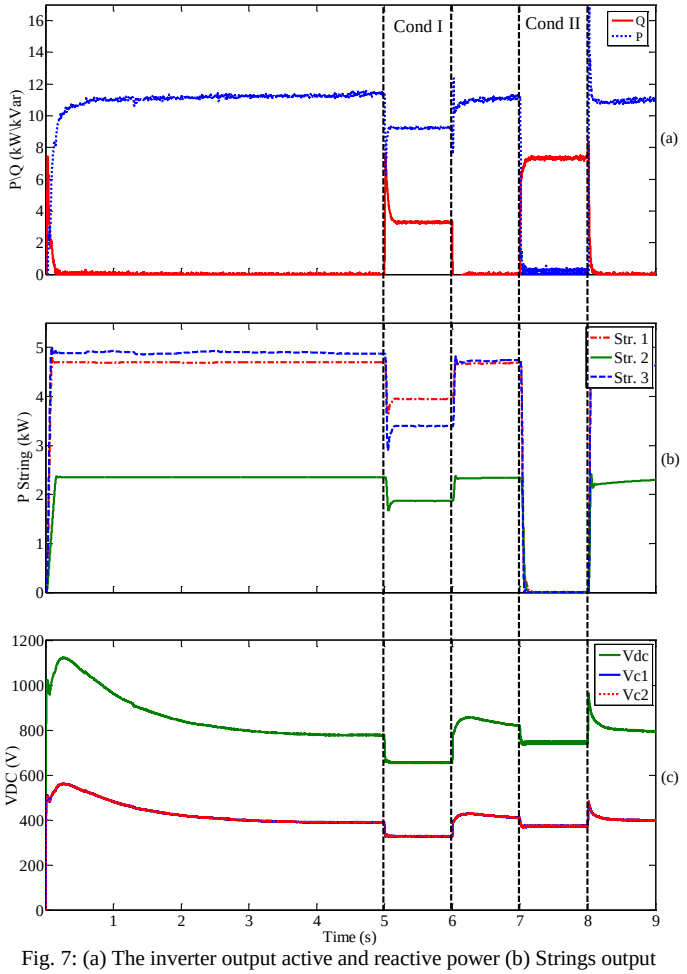

Fig. 7: (a) The inverter output active and reactive power (b) Strings output power and (c) DC-link voltage and DC capacitors voltage under Cond I and II.

Under normal grid operation in Fig. 6(a), the NPC inverter delivers only the active power (unity power factor operation) to the grid. However, there is phase difference between the voltage

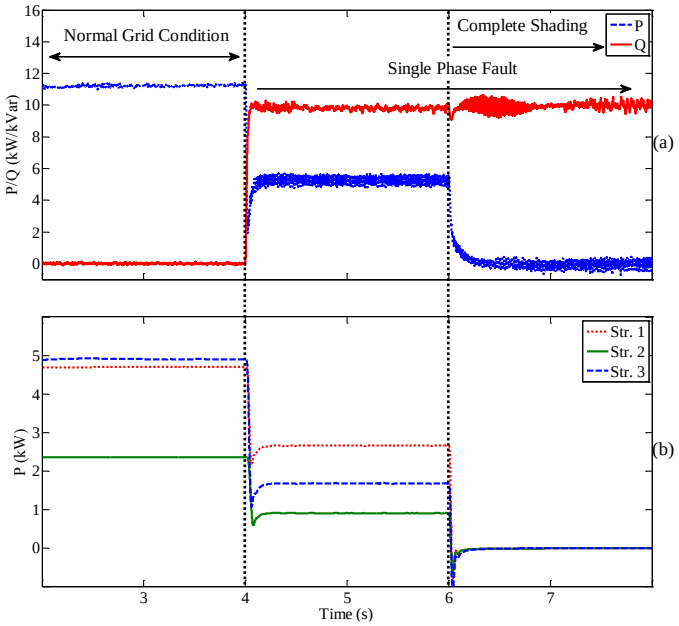

Fig. 8: FRT capability under complete shading of PV panels and Single phase voltage sag (54%): (a) Inverter active and reactive power and (b) Extracted power from strings.

and current for Cond. I. According to (1), the NPC inverter will deliver both active and reactive powers to the grid since the phase difference is less than $\pi/2$ *rad*. While the voltage magnitude of phases A and B is less than 0.5p.u for Cond. II in Fig. 6(b), the NPC inverter only injects reactive power to the grid. The amount of injected active and reactive power to the grid from the NPC inverter is shown in Fig. 7(a).

The dynamic performance of each PV string is also presented in Fig. 7(b). Since the PV strings experienced different irradiance and temperatures, they have different maximum power values. It should be noted that the total extracted PV power is decreased to zero in order to deliver pure reactive power to the grid for Cond. II. Besides that, the proposed control method maintained the V_{dc} during all fault conditions as shown in Fig. 7(c). The DC-link capacitor voltages are also remained balanced at all times. Moreover, the grid currents THD are less than 5% despite of any conditions.

In addition to that, the dynamic performance of the proposed control structure is also examined under total shading of PV panels as shown in Fig. 8. Before t = 4s, the grid is under normal operation where same amount of irradiance and temperature are received by the PV panels like those in Fig. 7. It can be observed that the amount of injected reactive power is zero in this condition. A single phase fault (phase B) experienced a 54% voltage sag during t = 4s at the point of the PV inverter connection. Hence, the controller of the NPC inverter must be changed in order to produce the adequate amount of reactive power to the grid. The inverter has injected both active and reactive power to the grid between t = 4s to 6s. However, the amount of injected active power is reduced according to the inverter current capability. Besides that, the extracted power of the PV strings is also decreased using the proposed DC/DC controller. At t = 6s, there is complete shading across all the PV

panels. Thus, there is zero power extracted as shown in Fig. 8(b). Nevertheless, the reactive power is still injected to the grid from the inverter despite of experiencing full PV shading. Thus, the results have proven the feasibility of the proposed controller which has also enhanced the quality of grid voltage by injecting reactive power in the event of any grid faults as well as complete PV shading.

Thus, the evaluation results have evidently proven that excellent FRT performance and dynamic response are achieved for the proposed multi-string PV plant in Fig. 1 under both balanced and unbalanced grid fault conditions. The proposed controller allows the PV power plant to stay connected to the grid even when the PV panels experienced full shading while improving the grid voltage quality during all fault conditions.

V. CONCLUSION

In this paper, the DC-link voltage control strategy is proposed for the DC/DC converter in the two-stage multi-string PV plant. The proposed control maintained the V_{dc} under any grid fault conditions by reducing the extracted PV power to match with the inverter output power. Meanwhile, the proposed VOC-PR controller injects the adequate amount of active and reactive power to the grid in order to improve the grid power quality under any grid fault conditions. On top of that, the ASVM method balanced well the DC-link capacitor voltages at all times.

Hence, the implementation of the proposed control has successfully overcome the issues of excessive DC-link voltage, increased grid currents and unbalanced capacitor voltages under any grid fault conditions. The evaluation results have also proven its feasibility. The precise and fast dynamic response of the proposed system with its enhanced FRT capability makes it attractive for large-scale PV plants. On top of that, the proposed controller even allows the PV power plant to remain connected to the grid at night.

VI. REFERENCES

[1] D. Feldman, "Photovoltaic (PV) pricing trends: historical, recent, and near-term projections," 2014.

[2] H.C. Chen, C.T. Lee, P.T. Cheng, R. Teodorescu, F. Blaabjerg, and S. Bhattacharya, "A flexible low-voltage ride-through operation for the distributed generation converters," in Power Electronics and Drive Systems (PEDS), 2013 IEEE 10th International Conference on, April 2013, pp. 1354–1359.

[3] H. Yamauchi, A. Yona, and T. Senjyu, "Design of FRT capability and distributed voltage control of PV generation system," in Power Electronics and Drive Systems (PEDS), 2011 IEEE Ninth International Conference on, Dec 2011, pp. 867–872.

[4] M. Mirhosseini, J. Pou, and V. Agelidis, "Single and two-stage inverter based grid-connected photovoltaic power plants with ride-through capability under grid faults," Sustainable Energy, IEEE Transactions on, no. 99, pp. 1–10, 2014.

[5] L. Chih-Ming, Y. Chung-Ming, Y. Wei-Shan, and L. Yung-Hsiang, "An LVRT control strategy for reducing DC-link voltage fluctuation of a two-stage photovoltaic multilevel inverter," in Power Electronics and Drive Systems (PEDS), 2013 IEEE 10th International Conference on, 2013, pp. 908-913.

[6] M. Kasper, D. Bortis, and J. Kolar, "Classification and comparative evaluation of PV panel-integrated DC-DC converter concepts," Power Electronics, IEEE Transactions on, vol. 29, no. 5, pp. 2511–2526, May 2014.

[7] N. Adhikari, B. Singh, and A. L. Vyas, "Performance evaluation of a low power solar-PV energy system with SEPIC converter," in Power Electronics and Drive Systems (PEDS), 2011 IEEE Ninth International Conference on, 2011, pp. 763-769.

[8] "IEEE standard for interconnecting distributed resources with electric power systems," IEEE Std 1547-2003, July 2003.

[9] Y. Yang and F. Blaabjerg, "Low-voltage ride-through capability of a single-stage single-phase photovoltaic system connected to the low voltage grid," International Journal of Photoenergy, vol. 2013, pp. 1-9, 2013.

[10] G. Mehta, S. P. Singh, and R. D. Patidar, "Grid interconnection of distributed generation system with power quality improvement features," in Power Electronics and Drive Systems (PEDS), 2011 IEEE Ninth International Conference on, 2011, pp. 329-333.

[11] E. O. GmbH., Grid code high and extra high voltage. [Online]. Available: http://www.eon-netz.com

[12] S. Kouro, K. Asfaw, R. Goldman, R. Snow, B. Wu, and J. Rodriguez, "NPC multilevel multistring topology for large scale grid connected photovoltaic systems," in Power Electronics for Distributed Generation Systems (PEDG), 2010 2nd IEEE International Symposium on, June 2010, pp. 400–405.

[13] A. I. Maswood, E. Al-Ammar, and F. Liu, "Average and hysteresis current-controlled three-phase three-level unity power factor rectifier operation and performance," Power Electronics, IET, vol. 4, pp. 752-758, 2011.

[14] D. P. Hohm and M. E. Ropp, "Comparative study of maximum power point tracking algorithms using an experimental, programmable, maximum power point tracking test bed," in Photovoltaic Specialists Conference, 2000. Conference Record of the Twenty-Eighth IEEE, 2000, pp. 1699-1702.

[15] R. Teodorescu, F. Blaabjerg, M. Liserre, and P. Loh, "Proportional resonant controllers and filters for grid-connected voltage-source converters, "Electric Power Applications, IEE Proceedings, vol. 153, no. 5, pp.750–762, September 2006.

[16] H. Pinkymol, A. Maswood, O. Gabriel, and L. Ziyou, "Analysis of 3-level inverter scheme with DC-link voltage balancing using LS-PWM and SVM techniques," in Renewable Energy Research and Applications (ICRERA), 2013 International Conference on, Oct 2013, pp. 1036–1041.

[17] H. R. Pinkymol, A. I. Maswood, and A. Venkataraman, "Space vector based field oriented control of Permanent Magnet Synchronous Motor with a 3-level inverter scheme," in Transportation Electrification Conference and Expo (ITEC), 2013 IEEE, 2013, pp. 1-6.